First-principles study of the phonon replicas in the photoluminescence spectrum of 4H-SiC

Sai Lyu and Walter R. L. Lambrecht

Phys. Rev. B **101**, 045203 — Published 15 January 2020

DOI: 10.1103/PhysRevB.101.045203

First-principles study of the phonon replicas in the photoluminescence spectrum of 4H-SiC

Sai Lyu* and Walter R. L. Lambrecht
Department of Physics, Case Western Reserve University, 10900 Euclid Avenue, Cleveland, Ohio 44106-7079, USA

The free-exciton photoluminescence (PL) spectrum of 4H-SiC exhibits a detailed fine structure due to the different phonons involved in the indirect gap transition. Here a first-principles calculation of these phonons, their symmetry labeling and their contribition to the photoluminescence spectrum is presented. The calculation uses phonons and electron-phonon coupling matrix element computed via density functional perturbation theory and energy bands and optical phonon matrix elements calculated in density functional theory. The results are in excellent agreement with experiment for the phonon energies and the polarization dependence of the spectrum. The relative intensities are also in fair agreement if we allow for some phonons within a few meV to be interchanged. There is however a remarkable discrepancy that the experimental spectrum shows a distinct behavior for phonons with energy below ~ 55 meV and above that energy, which is absent in the theory. The experimental PL lines corresponding to phonon energies below 55 meV are about a factor 5-10 smaller in intensity. This is not found in our calculations. The calculations show a similar peak distribution as the experiment in this range but with intensities comparable to those above 55 meV. This indicates that another mechanism outside the scope of the electron-phonon mediated transitions is operative for photon energies of the PL lines closer to the indirect exciton gap than this 55 meV cut-off, which reduces the overall intensity of these lines. We propose that this may result from competition between the phonon-assisted PL and trapping of the electron in the available unoccupied hexagonal site N-donor shallow level at 53 meV binding energy. As part of this study, we also present the phonon dispersions and density of states in 4H-SiC and the electronic band structure including quasiparticle corrections.

I. INTRODUCTION

Photoluminescence (PL) is a light-emission process in which solids (or molecules) radiate photons as a consequence of recombination of electron-hole pairs. These electron-hole pairs are created by exciting light. The PL technique can also be used to identify phonons in indirect gap semiconductors. This is because the PL spectrum in indirect gap semiconductor corresponds to a second-order transition process assisted by phonon absorption or emission. In indirect gap materials where the valence band maximum (VBM) and conduction band minimum (CBM) occur at different points in the Brillouin zone, direct transitions due to the photon field alone are forbidden by momentum conservation and the fact that visible light has negligible momentum compared to the Brillouin zone dimensions.

4H-SiC is well known to have an indirect band gap between the VBM at Γ and the CBM at the points M of the hexagonal Brillouin zone. Because of the large size of the unit cell, consisting of 4 layers, the phonon spectrum is rather complex and leads to fine structure of the band gap exciton PL, known as the phonon replicas. These spectra were already reported in 1965 by Patrick *et al.* [1] and used in an attempt to determine the **k**-space location of the conduction band minimum although that paper used the donor-bound excitons (for a N-impurity on a hexagonal C-site), the so-called P-lines. Using symmetry arguments and the limited information at that time on the phonons based on folding of a simple assumed phonon dispersion led them to the conclusion that the conduction band minimum could not be at M but had to be in between M and L. This was in contrast with first-principles band structure calculations performed later on and the issue was resolved in Ref. 2 by using the phonon spectra that had been reported by then by Hoffmann *et al.* [3]. A satisfactory fit of the P-series phonon replicas with the phonon data was reported by Choyke *et al.* [4]. The phonon replica spectrum based on the free exciton I-lines has more recently been reported by Ivanov *et al.* [5]. The relative intensity of the P and I lines depends on the degree of N-doping. Although that study already included an analysis in terms of the phonon spectrum, it was based on a semi-empirical model for the force constants and symmetry analysis. A full first-principles description has not yet been provided. More recently, the phonon replicas have also been measured by high-resolution differential absorption by Klahold *et al.* [6].

Here, we adapt a first-principles formalism recently used for indirect absorption[7] to simulate the PL spectrum in indirect gap semiconductors. This formalism is based on density functional theory (DFT) and density functional perturbation theory (DFPT) for the phonons and electron-phonon coupling matrix elements. We apply this approach to the case of 4H-SiC and compare our theoretical calculations with available experimental results. Although the measured spectrum corresponds to

* Current address: Chaire de Simulation à l' Échelle Atomique (CSEA), École Polytechnique Fédérale de Lausanne, 1015 Lausanne, Switzerland

excitons, we here neglect the electron-hole interaction or exciton binding energy. In other words, we view the PL replicas as a recombination of a free CBM electron with a free VBM hole via different phonons without taking into account that the electron and hole start out from a bound exciton state. Nonetheless, it is the clear separation of the exciton state from the continuum of the band that allows us to treat the transitions as well defined discrete energies with a simple lineshape not requiring an integration over **k**-points near the band extrema.

II. COMPUTATIONAL METHOD

The approach used here to treat indirect transitions is similar to the one recently introduced by Noffsinger *et al.* [7] for the calculation of the indirect absorption in Si. The difference is that instead of integrating over the Brillouin zone, we here focus on the phonon-assisted recombination between only the **k**-points corresponding to the minimum indirect gap.

The process considered here corresponds to the recombination of a free electron at the conduction band minimum (CBM) (at the M points in 4H-SiC) with a free hole at the valence band maximum (VBM) (at the Γ point). This is a second-order process involving a phonon and a photon so that both energy and momentum are conserved. The perturbation Hamiltonian due to electron-photon interaction and electron-phonon interaction can be expressed as

$$\Delta H = H^r + H^{ep} \tag{1}$$

where $H^r = (-e/cm)\mathbf{p}\cdot\mathbf{A}$ is the radiation Hamiltonian in the momentum gauge with $\mathbf{E} = E\hat{\epsilon} = -i(\omega/c)\mathbf{A}$ the electric field with polarization $\hat{\epsilon}$. We prefer here the momentum or velocity gauge rather than the length gauge because for periodic solids the matrix elements of the position operator between Bloch functions require special care[8]. On the other hand, H^{ep} is the electron-phonon interaction Hamiltonian

$$H^{ep} = \frac{1}{\sqrt{N}}\sum_{\mathbf{k},\mathbf{q},mn\nu} g_{mn\nu}(\mathbf{k},\mathbf{q}) c^\dagger_{m\mathbf{k}+\mathbf{q}} c_{n\mathbf{k}} (a_{\mathbf{q}\nu} + a^\dagger_{-\mathbf{q}\nu}) \tag{2}$$

written in second quantization form with $c_{n\mathbf{k}}$ the electron annihilation and $a_{\mathbf{q}\nu}$ the phonon annihilation operator for mode ν at wavevectro $\mathbf{q}$ and N the number of unit cells in the crystal using periodic boundary conditions. The electron-phonon coupling matrix elements are

$$g_{mn\nu}(\mathbf{k},\mathbf{q}) = \langle m\mathbf{k}+\mathbf{q}|\partial_{\mathbf{q}\nu} V^{KS}|n\mathbf{k}\rangle_{uc} \tag{3}$$

which couples the electron Bloch state $|n\mathbf{k}\rangle$ to state $|m\mathbf{k}+\mathbf{q}\rangle$ and the integral is taken over the unit cell. It involves the first order change in the Kohn-Sham potential in response to the phonon mode $\mathbf{q}\nu$ written as $\partial_{\mathbf{q}\nu}V^{KS}$. This can in turn be written in terms of the derivatives of the Kohn-Sham potential as a function of individual atomic displacements τ_α of atom τ in the Cartesian direction α and the phonon eigenvector:

$$\partial_{\mathbf{q}\nu} V^{KS}(\mathbf{r}) = l_{\mathbf{q}\nu}\sum_{\tau\alpha}\left(\frac{M_0}{M_\tau}\right)^{1/2} e_{\tau\alpha,\nu}(\mathbf{q})\partial_{\tau\alpha,\mathbf{q}} V^{KS}(\mathbf{r}) \tag{4}$$

with $l_{\mathbf{q}\nu} = \sqrt{\hbar/(2M_0\Omega_{\mathbf{q}\nu})}$ the characteristic length of the particular phonon with frequency $\Omega_{\mathbf{q}\nu}$ using an arbitrary reference mass M_0 and

$$\partial_{\tau\alpha,\mathbf{q}} V^{KS}(\mathbf{r}) = \sum_{\mathbf{T}} e^{-i\mathbf{q}\cdot(\mathbf{r}-\mathbf{T})}\frac{\partial V^{KS}}{\partial\tau_\alpha}(\mathbf{r}-\mathbf{T}) \tag{5}$$

The phonon eigenvector is the eigenvector of the dynamical matrix:

$$\sum_{\tau'\alpha'} D_{\tau\alpha,\tau'\alpha'} e_{\tau'\alpha',\nu}(\mathbf{q}) = \Omega^2_{\mathbf{q}\nu} e_{\tau\alpha,\nu}(\mathbf{q}) \tag{6}$$

For details of the formalism and how the matrix elements are obtained in DFPT see for example the review article by Giustino [9].

The transition rate from inital state $|i\rangle$ of an electron at the CBM at M and the ground state of the vibrational system, to the final state $|f\rangle$ with an electron at the VBM (here at Γ) and one phonon emitted is obtained in second order perturbation theory involving each of the interaction Hamiltonians once and is given by a Fermi's Golden Rule like formula:

$$w_{fi}(\omega) = \frac{2\pi}{\hbar}\sum_\nu \left| \sum_{m_1} \frac{\langle f|H^r|m_1\rangle\langle m_1|H^{ep}|i\rangle}{\varepsilon_i - \varepsilon_{m_1} - \hbar\Omega_{\mathbf{q}\nu}} + \sum_{m_2}\frac{\langle f|H^{ep}|m_2\rangle\langle m_2|H^r|i\rangle}{\varepsilon_i - \varepsilon_{m_2} - \hbar\omega}\right|^2 \times\delta(\varepsilon_f - \varepsilon_i + \hbar\omega + \hbar\Omega_{\mathbf{q}\nu}). \tag{7}$$

Here the matrix element of the H^{ep} corresponds to $\langle m_1|H^{ep}|i\rangle = g_{m_1 i\nu}(\mathbf{k}_i,\mathbf{q})$ in the first term and the intermediate state m_1 is at $\mathbf{k}_i+\mathbf{q}=\mathbf{k}_f$. The matrix element of H^r is between the intermediate state m_1 and the final state at the final $\mathbf{k}_f$ and is a vertical momentum matrix element. Using $\mathbf{p} = m\mathbf{v}$, we write it instead in terms of velocity matrix elements:

$$\langle f|H^r|m_1\rangle = \langle f|\hat{\epsilon}\cdot\mathbf{v}|m_1\rangle|E|/\omega \tag{8}$$

The magnitude of the electric field $|E|^2$ ultimately corresponds to the energy density of the electromagnetic field and is a factor of no interest here because we are not deriving the absolute emission rate but only the relative intensity of transitions involving different phonons. The overall factor $1/\omega^2$ resulting from each velocity matrix element modulo squared varies little over the range of interest and can therefore be ignored. Similarly, in the second term, m_2 is a state at $\mathbf{k}_i$ and involves a vertical velocity matrix element at the initial $\mathbf{k}_i$ and $\langle f|H^{ep}|m_2\rangle = g_{fm_2\nu}(\mathbf{k}_i,\mathbf{q})$. We assumed here that because at low temperature, there are few (or no) phonons

present initially, the dominant process involves phonon emission and hence it is the sum of the phonon and photon energy $\hbar(\Omega_{\mathbf{q}\nu} + \omega)$ that must equal the band gap $\varepsilon_f - \varepsilon_i$. The phonons involved correspond obviously to the $\mathbf{q}$ point connecting the initial to the final band state, so here the phonons at M.

The equation for the optical absorption coeffcient given in Ref. 7 can be derived from the above but would interchange the role of the initial and final states. Also, from the absorption coefficient, one can obtain the spontaneous emission coefficient using the Einstein relation between spontaneous emission and stimulated absorption involving the blackbody distribution coefficient. Compared to our expression for the transition rate, which has a common factor $1/\omega^2$, the absorption coefficient has a prefactor of $1/[\omega n(\omega)]$ with n the index of refraction and for the emission coefficient this would be multiplied by a factor ω^3. We ignore here these factors because over the range of the phonons involved, they vary little. In the present expression for the transition rate, we do not include the Fermi-Dirac distribution factor because the conduction band is occupied and a hole is assumed to be present in the valence band by the initial process of exciting the electron hole pairs and subsequently letting them thermalize to the band edges. We also do not need to include phonon occupation numbers because at low temperature we only need to take into account phonon emission.

A few other remarks are in order when applying these equations to the specific case of 4H-SiC. The final state f is the two fold degenerate VBM of Γ_5 symmetry. Thus the contributions of both eigenvectors used as the basis in the corresponding two-dimensional vector space must be added. So, there is a sum over the two f states outside the $|\dots|^2$ in Eq.(7). We here neglect the spin-orbit splitting of the VBM which is of order 7 meV. There are also 3 equivalent initial state M-points in the Brillouin zone that contribute. These need to be summed over and here again we assume that this sum can be done over the absolute values modulo squared rather than adding the amplitudes coherently. Although, in principle, the exciton could be a coherent superposition of the contributions from the three M-valleys, we here assume that excitons from each valley recombine independently of each other. We have verified that each of the three M-points gives the same contribution for $E \parallel c$ and for the $E \perp c$ case this amounts to a symmetrizing average ensuring that the final result is isotropic in the c-plane.

The calculations are performed using the ABINIT package [10] using Hartwigsen-Goedecker-Hutter (HGH) pseudopotentials [11]. We employ a $8 \times 8 \times 2$ $\mathbf{k}$-point mesh and the plane wave energy cutoff is set as 80 Ha. The electronic band structure are calculated at the level of DFT in the LDA. The velocity matrix elements are obtained from the ABINIT parts for optical absorption calculations involving direct interband transitions by using the printed out matrix elements only at the two specific $\mathbf{k}$-points we need here. Note that they are not equal to the momentum matrix elements divided by the electron mass because of the non-local part of the pseudopotential, which does not commute with the Hamiltonian. The electron-phonon coupling matrix elements are also provided by the ABINIT code and are calculated as explained in Ref. 9. The phonon frequencies and eigenvectors needed in here are obtained in DFPT from the ABINIT code. We note that, in principle, in these expressions there is no limitation on the intermediate states, so $f = m_1$ and $i = m_2$ should be included. However, these intra-band matrix elements of the velocity operator reduce simply to the band velocity $\nabla_{\mathbf{k}} E_n(\mathbf{k})/\hbar$, which is zero for all the bands at Γ and M.

For the electronic band structures, we also use the energy bands calculated in the LDA by ABINIT. However, we also can use the more accurate band structure energies obtained in the quasiparticle self-consistent GW or QSGW method [12, 13] where G stands for the one-particle Green's function and W for the screened Coulomb interaction [14, 15]. In the GW calculations, we use a $spdf-spd$ basis set, Σ is calculated up to 2.5 Ry and self energy is approximated by a diagonal average matrix when above 2 Ry. A 3.5 Ry interstitial plane-wave cutoff is used for Columb interactions and basis functions.In contrast to the LDA, which is well known to underestimate the band gaps severely, this method typically only slightly overestimates the band gaps because of the underscreening of W in the random phase approximation. This can be corrected by incuding only 80% of the self-energy correction to the LDA exchange and correlation potential [16]. We will show that for present purpose including the GW corrections to the bands does not make a significant change for the phonon replica spectrum.

III. RESULTS

A. Crystal structure and symmetry

The crystal structure of 4H-SiC is shown in Fig. 1. In cartesian coordinates, the three lattice vectors can be expressed as

$$\begin{aligned} \mathbf{a}_1 &= a(\frac{\sqrt{3}}{2}, \frac{1}{2}, 0) \\ \mathbf{a}_2 &= a(0, -1, 0) \\ \mathbf{a}_3 &= c(0, 0, -1) \end{aligned} \tag{9}$$

The relaxed lattice constants a and c are given in Table I and comparisons are made to the available results in literature. Our relaxed lattice constants slightly underestimate experimental ones as is usually the case for LDA. There are four atomic double layers perpendicular to the c axis. Each double layer is composed of one pure Si layer and C layer. Each Si atom is surrounded by four C atoms forming a tetrahedron and *vice versa* for the C atom.

The space group is C_{6v}^4 which contains 12 symmetry operations in the corresponding point group. The group

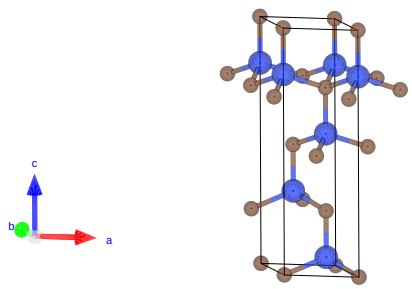

FIG. 1. The crystal structure of 4H-SiC. The smaller brown spheres and larger blue spheres denote C atoms and Si atoms respectively. Note that there are 8 atoms per cell, 4 Si-C pairs in ABCA stacking. The atoms included in the figure occurring in neighboring cells are shown to emphasize the tetrahedral coordination.

TABLE I. Lattice parameters of 4H-SiC.

	a(Å)	c(Å)
This work	3.048	9.978
Ref.[17]	3.067	10.032
Expt.[18]	3.073	10.052

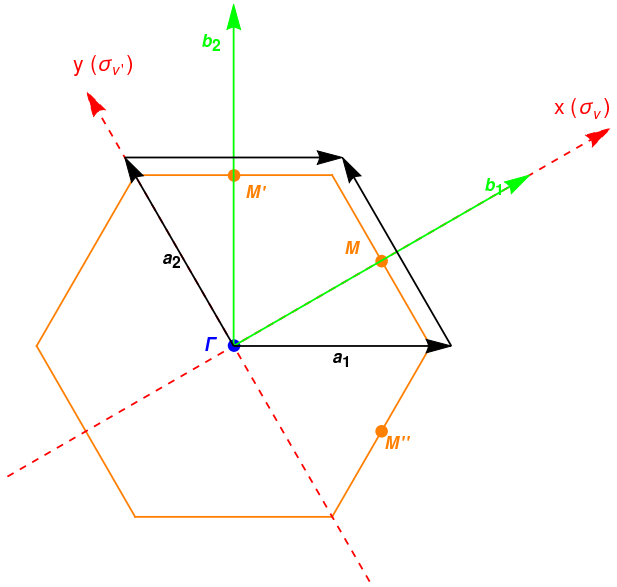

FIG. 2. Projection of the Brillouin zone on the c-plane with reciprocal lattice vectors $\mathbf{b}_1$, $\mathbf{b}_2$, in relation to the real space primitive vectors: $\mathbf{a}_1$, $\mathbf{a}_2$. Of the three equivalent M, M', M'' points, the M-point along the $\mathbf{b}_1$ direction, which coincides with Cartesian x axis is the one used to give the optical matrix elements in the Appendix. The mirror planes and x,y axes are shown in dashed red lines.

of $\mathbf{k}$ at the M point in the Brillouin zone is C_{2v}, which includes 4 symmetry operations. It is used to label the relevant phonons. We use the same character table as in Ref. 5.

The symmetry operations of the point group C_{2v} at the M point are indicated in Fig. 2. There are three independent M points in the centers of the sides of the hexagonal Brillouine zone (not connected by a reciprocal lattice vector). As already mentioned above, their contributions are added, which results in an isotropic intensity in the c-plane. The mirror planes at one of the M-points are shown in Fig. 2. They define the symmetry labeling: M_1 and M_2 states are even under σ_v in the xz-plane while M_3 and M_4 are odd. M_1 and M_3 irreducible representations are even under the two-fold rotation about the z-axis and M_2 and M_4 are odd. Thus M_1 behaves as z, M_4 as x, M_2 as y and M_3 as xy.

B. Electronic band structure

In Fig. 3, we show the LDA electronic band structure of 4H-SiC calculated by ABINIT. 4H-SiC is found to have an indirect gap (M-Γ) of 2.21 eV in LDA, compared with the experimental value [19] of the exciton gap of 3.2664 eV. The exciton binding energy is small compared to this discrepancy and clearly not the major issue. The Kohn-Sham eigenvalues and corresponding symmetry labels at the Γ and M points are given in Table II. Our results

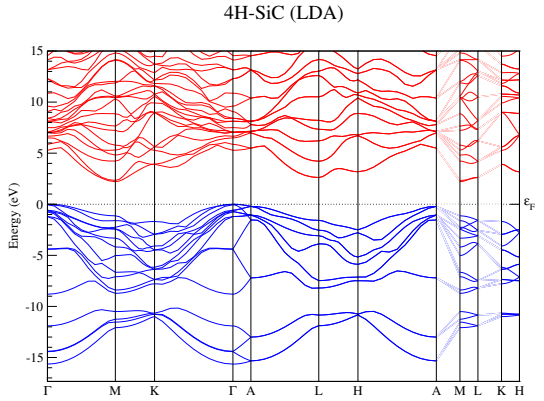

FIG. 3. The LDA band structure of 4H-SiC.

are in accord with previous calculations by Persson *et al.* [17]. Those Kohn-Sham eigenvalues are used in the energy denominators in Eq.(7). For comparison, the band structure calculated in the QSGW 0.8Σ approximation are given in Fig. 4 and the relevant eigenvalues at Γ and M obtained in this method are also included in Table II. In this approximation, the indirect band gap is found to be 3.20 eV in excellent agreement with experiment to within 0.1 eV. We have also used these band energies in the calculation of the indirect transitions. While it is not entirely consistent to use QSGW bands combined with LDA calculated matrix elements, it allows us at least to check to what extent the band energies used modify intensities. We will show it has little effect.

TABLE II. Symmetry label and energies (in eV relative to the VBM) of the electronic band structure at Γ and M points.

band	at $\Gamma(C_{6v})$			at $M(C_{2v})$		
	DFT	QSGW	sym	DFT	QSGW	sym
$Ev16$	-15.64	-15.94	Γ_1	-12.08	-12.51	M_1
$Ev15$	-14.43	-14.75	Γ_4	-11.53	-11.98	M_4
$Ev14$	-14.40	-14.70	Γ_4	-11.25	-11.73	M_4
$Ev13$	-11.91	-12.36	Γ_1	-10.50	-11.00	M_1
$Ev12$	-8.80	-9.00	Γ_1	-8.72	-8.96	M_4
$Ev11$	-4.41	-4.67	Γ_4	-8.40	-8.66	M_1
$Ev10$	-4.37	-4.63	Γ_4	-7.09	-7.44	M_1
$Ev9$	-1.20	-1.31	Γ_5	-6.66	-7.02	M_4
$Ev8$	-1.20	-1.31	Γ_5	-5.02	-5.18	M_1
$Ev7$	-0.73	-0.80	Γ_6	-4.18	-4.33	M_4
$Ev6$	-0.73	-0.80	Γ_6	-3.32	-3.51	M_2
$Ev5$	-0.59	-0.65	Γ_6	-2.43	-2.57	M_3
$Ev4$	-0.59	-0.65	Γ_6	-2.41	-2.56	M_3
$Ev3$	-0.05	-0.004	Γ_1	-2.25	-2.36	M_4
$Ev2$	0.00	0.00	Γ_5	-1.60	-1.67	M_1
$Ev1$	0.00	0.00	Γ_5	-1.13	-1.23	M_2
$Ec1$	5.29	6.07	Γ_1	2.21	3.20	M_4
$Ec2$	5.86	6.71	Γ_4	2.33	3.34	M_1
$Ec3$	6.50	7.22	Γ_4	4.23	5.29	M_4
$Ec4$	6.66	7.36	Γ_1	4.82	5.77	M_1
$Ec5$	7.05	8.16	Γ_5	5.31	6.45	M_4
$Ec6$	7.05	8.16	Γ_5	5.78	7.00	M_1
$Ec7$	7.05	8.24	Γ_6	7.23	8.45	M_2
$Ec8$	7.05	8.24	Γ_6	7.66	8.86	M_1
$Ec9$	7.50	8.60	Γ_1	8.86	10.02	M_4
$Ec10$	8.13	9.34	Γ_5	10.33	11.44	M_4
$Ec11$	8.13	9.34	Γ_5	10.43	11.57	M_1
$Ec12$	8.41	9.57	Γ_6	10.50	11.75	M_3
$Ec13$	8.41	9.57	Γ_6	10.58	11.84	M_3
$Ec14$	9.07	10.16	Γ_4	11.87	13.07	M_4
$Ec15$	9.61	10.74	Γ_4	12.03	13.35	M_1
$Ec16$	10.87	12.24	Γ_1	14.09	15.29	M_2
$Ec17$	12.30	13.74	Γ_5	14.16	15.38	M_4
$Ec18$	12.30	13.74	Γ_5	14.81	16.05	M_1
$Ec19$	13.16	14.61	Γ_6	15.21	16.49	M_1
$Ec20$	13.16	14.61	Γ_6	16.73	18.27	M_1
$Ec21$	14.13	15.64	Γ_4	16.88	18.28	M_4
$Ec22$	14.55	16.22	Γ_1	17.18	18.58	M_2
$Ec23$	15.95	17.31	Γ_6	17.61	19.00	M_3
$Ec24$	15.99	17.31	Γ_6	17.84	19.24	M_3

C. Phonon dispersion and density of states

The phonon dispersions and phonon density of states are shown in Fig. 5. The discontinuities at the Γ point are due to the fact that in this plot the LO-TO splitting at Γ is not included, only the TO mode. So, the LO branch suddenly changes to the TO mode at the Γ-point. The LO modes at Γ depend on which direction one approaches Γ from. In the phonon density of states we can see that the higher optical modes are dominated by the lower mass C-atom.

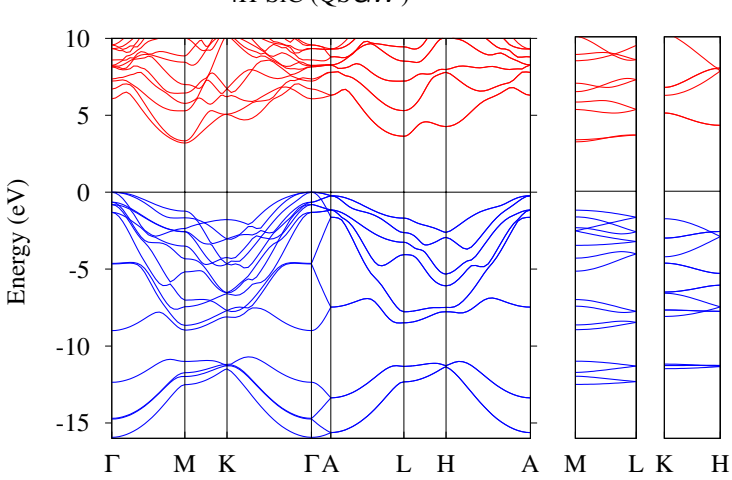

FIG. 4. The QSGW band structure of 4H-SiC.

D. Phonon modes at the M point

The phonon modes relevant to the present calculation of the PL spectra are the modes at M and are given in Table III. For each mode we give our calculated phonon energy in meV, the corresponding values from Ivanov *et al.* [5], and from Klahold *et al.* [6], the symmetry label according to the irreducible representations of the C_{2v} point group and the light polarization for which this phonon mode gives allowed transitions. M_2 and M_4 correspond to $E \perp c$, while M_1 and M_3 correspond to $E \parallel c$. We can see that the calculated and the observed phonon frequencies agree generally to within ±2 meV. We re-ordered a few of the experimentall observed phonon frequencies to match as closely as possible with our calculated ones based on their polarization. Note that our calculated M_3 phonon at 94.5 meV and M_1 mode at 95.5 meV may be hidden in the experimental 94.7 mode for $E \parallel c$ which is the strongest peak in the experiment. We have indicated this in the Table III with the question marks. It matches very well with our calculated M_3 mode at 94.8 meV which indeed we also find to have the highest intensity among all $E \parallel c$ modes. The experimental peak reported at 109.5 meV does not match any of our modes and is in fact very weak in experiment. Some of the peaks from Ref. [6] are labeled as corresponding to transitions from the spin-orbit split-off valence band to the conduction band, *e.g.* 94.5+6.8 (SO) or 96.0+7.1 (SO) for $E \perp c$. While we do not question this interpretation, we note that 96.0+7.1=103.1 is also close to our calculated 103.6 meV for $E \perp c$ and so both the top valence band and a phonon at $\sim 103 \pm 1$ meV and the spin-orbit split-off VB with a slightly lower phonon could contribute to the same experimental peak.

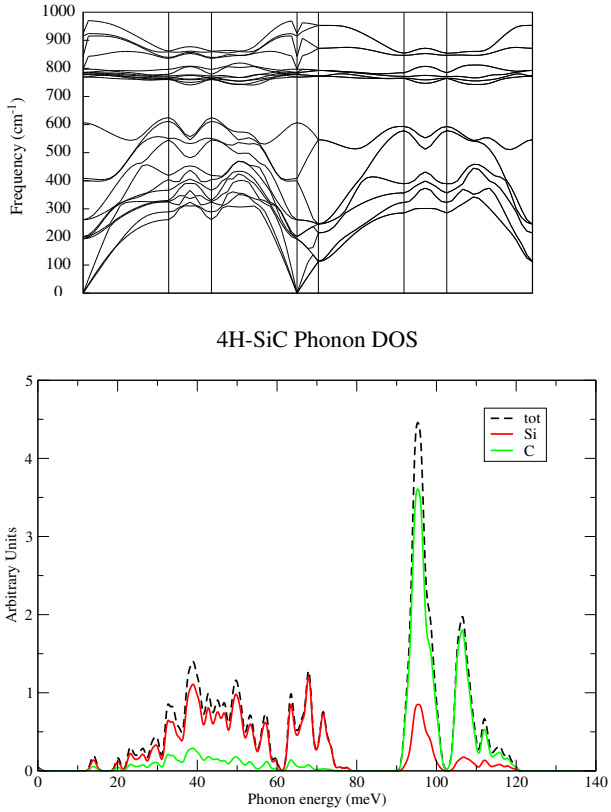

FIG. 5. The phonon dispersion along different **k**-directions and phonon density of states of 4H-SiC.

E. Symmetry considerations for optical and electron-phonon coupling matrix elements

For $E \parallel c$ and for the vertical matrix elements at M we note that because a vector along z or **c** belongs to the irreducible representation M_1 and the CBM is of symmetry M_4 the only non-zero matrix elements occur with the M_4 symmetry electronic energy bands. For $E \perp c$ we note that for the M-point lying in the x-direction, the M_4 states have the same symmetry as a vector along x. For an optical matrix element with polarization along x, then only the M_1 band states give a non-zero contribution (because $M_4 \otimes M_4 = M_1$) and for polarization along y, which corresponds to M_2 only $M_4 \otimes M_2 = M_3$ bands contribute.

As for optical matrix elements at the final state Γ that can couple to the VBM, of Γ_5 symmetry, we have that for $E \parallel c$ which belongs to Γ_1 only Γ_5 states can contribute non-zero matrix elements but for $E \perp c$ the velocity vector lies in the xy-plane and thus belongs to Γ_5. Since $\Gamma_5 \otimes \Gamma_5 = \Gamma_1 \oplus \Gamma_2 \oplus \Gamma_6$, all the latter three symmetry bands can contribute.

We have verified that these rules are obeyed by the matrix elements and give their numerical values in Appendix A for the M-point.

We now consider the electron-phonon coupling matrix elements that link the intermediate states at M to the Γ_5 VBM. For $E \parallel c$ these are only the M_4 states as mentioned above. Now, when an M_4 band state is combined with a M_1 phonon the overall symmetry is M_4 and hence x-like for the M-point in the x-direction. This is compatible with the Γ_5 symmetry of the final state, the VBM. For a M_3 phonon, we obtain $M_4 \otimes M_3 = M_2$ which is y-like and that is also compatible with Γ_5, so we see indeed that both M_1 and M_3 phonons will be allowed for $E \parallel c$. Likewise for $E \perp c$, the band states at M to consider are of symmetry M_1 and M_3. A phonon of M_2 symmetry combined with a band state of M_1 gives $M_1 \otimes M_2 = M_2$ which is y-like, while for a band of M_3 symmetry the combined state has $M_3 \otimes M_2 = M_4$ (which is x-like). Both or these are compatible with the irreducible representation Γ_5 of the VBM. The same is true for a M_4 symmetry phonon but now the role of x and y are reversed.

For electron-phonon coupling linking the intermediate states at Γ with the CBM of M_4 similar considerations apply. For example, for $E \parallel c$ only Γ_5 intermediate states need to be considered and these being x or y like they have non-zero matrix elements with the M_4 conduction band for phonons of symmetry M_1 or M_3. For $E \perp c$ intermediate states can have Γ_1, Γ_2 or Γ_6 symmetry. For Γ_1 states, only phonon modes of symmetry M_4 can link to the M_4 CBM. An M_2 vibrational mode will link the

TABLE III. Calculated phonon energies (in meV) with symmetry labels at the M point of 4H-SiC and comparison with results from Ivanov *et al.* [5] and Klahold *et al.* [19]. The value after the + notation corresponds to the spin-orbit splitting of the VBM and indicates the assignment by Klahold *et al.* . The ? indicates tentative assignments.

This work	label	Ref. [5]	Ref.[6]	polarization
32.5	M_4	33.2	33.2	$E \perp c$
35.9	M_1	36.6	36.6	$E \parallel c$
40.3	M_2	41.1	41.1	$E \perp c$
40.5	M_3	40.6	40.6	$E \parallel c$
40.9	M_3	41.9	41.9	$E \parallel c$
45.4	M_4	46.3	46.3	$E \perp c$
50.1	M_2	50.9	50.9	$E \perp c$
51.9	M_1	52.7	52.7	$E \parallel c$
67.6	M_2	68.1	68.1	$E \perp c$
68.2	M_1	68.8	68.8	$E \parallel c$
75.8	M_1	78.2	78.0	$E \parallel c$
77.5	M_2	76.3	76.3	$E \perp c$
94.3	M_4	94.5	94.5	$E \perp c$
94.5	M_3	94.7?		$E \parallel c$
94.8	M_3	94.7	94.7	$E \parallel c$
94.8	M_4	94.5?	94.5?	$E \perp c$
95.5	M_1	94.7?		$E \parallel c$
95.9	M_2	96.0	96.0	$E \perp c$
96.7	M_1	96.5	96.5	$E \parallel c$
98.8	M_2	98.9	94.5+6.8	$E \perp c$
103.6	M_1	103.5	96.5+7.7	$E \parallel c$
104.2	M_2	103.9	96.0+7.1	$E \perp c$
106.6	M_1	106.3	106.3	$E \parallel c$
106.8	M_2	106.8	106.8	$E \perp c$
		109.5		$E \parallel c$

TABLE IV. Calculated intensity (in arbitrary units) of the photoluminescence at each phonon mode when $E \parallel c$.

Phonon energies	label	relative intensity (DFT eigenvalues)	relative intensity (GW eigenvalues)
35.9	M_1	21.83	21.91
40.5	M_3	1.00	0.49
40.9	M_3	0.10	0.10
51.9	M_1	1.31	1.32
68.2	M_1	3.53	3.49
75.8	M_1	14.75	13.62
94.5	M_3	9.46	11.17
94.8	M_3	25.24	21.32
95.5	M_1	0.34	0.10
96.7	M_1	26.35	25.26
103.6	M_1	0.40	0.42
106.6	M_1	14.75	11.95

TABLE V. Calculated intensity (in arbitrary units) of the photoluminescence at each phonon mode when $E \perp c$.

Phonon energies	label	relative intensity (DFT eigenvalues)	relative intensity (GW eigenvalues)
32.5	M_4	0.29	0.37
40.3	M_2	81.75	66.05
45.4	M_4	3.91	3.35
50.1	M_2	80.15	80.18
67.6	M_2	5.06	2.23
77.5	M_2	50.73	38.12
94.3	M_4	30.95	35.05
94.8	M_4	21.35	19.71
95.9	M_2	14.24	14.24
98.8	M_2	21.46	9.71
104.2	M_2	17.04	17.84
106.8	M_2	23.85	28.51

M_4 CBM state to an overall symmetry of M_3 which is behaves like a xy product and should thus couple to a Γ_6 intermediate state. A Γ_2 state on the other hand behaves like a rotation about the z axis and this cannot be turned in to M_4 by any phonon at M.

F. Simulated photoluminescence spectrum

The calculated relative intensity of the PL spectra for polarizations $E \parallel c$ and $E \perp c$ are presented in Table IV and V, respectively.

The simulated PL spectra for polizations $E \perp c$ and $E \parallel c$ are shown in Fig. 6 and are compared with the experimental data of Ivanov *et al.*[5], reproduced here. The width of each peak in the PL spectra is related to the lifetime of the phonon mode. It is presently not calculated. Here we use the same broadening factor (of 0.5 eV) for each phonon mode for simplicity. First we note that we calculated these either with the *GW* or with the LDA bands and both give very similar relative intensities as is clear from Tables IV,V and from comparison of the dashed cyan (*GW*) and violet solid lines (LDA). The experimental spectra show both free exciton (FE) I-lines and N-donor bound exciton (N-BE) (P and Q) lines. The relative intensity of P, Q, I lines depends on the concentration of N-impurites in the sample and on the interaction strength of the excitons with the impurities as discussed in Ivanov *et al.* [5]. We here include in dark green the spectrum dominated by P and Q lines from their paper to help see which lines are P lines and which are I-lines. The exciton binding energy to the hexagonal N-donor amounts to about 9 meV as can be seen from the shift of corresponding lines involving the same phonon in the indirect recombination. This agrees well with the value of 7 meV reported by Patrick *et al.* [1]. We thus shifted our calculated spectrum by 9 meV and reduced its intensity by a somewhat arbitrarily chosen factor to simulate the P-lines. This is shown by the blue lines in Fig. 6. The experimental peaks are labeled by I or P and the corresponding experimental phonon energies.

We note that in the experiments the peaks with phonon energies below about 55 meV are all much weaker than in the energy range above it. The experimental spectrum in this range was thus multiplied by a factor 10 for $E \parallel c$ to make it better visible and this is here shown by the red and orange lines. The calculated spectra show a qualitative agreement but with significant discrepancies with experiment.

Let us first discuss the $E \parallel c$ case. As mentioned already, it seems plausible that the strong modes at 94.5, 94.8 and weak one at 95.5 meV for $E \parallel c$ all correspond to the experimental 94.7 meV peak and their intensities should be added. We thus see good agreement of the largest peak with the experimentally largest peak. However, the calculated peak at 96.7 meV is much stronger than the experimental $I_{96.5}$ peak. The calculated 75.8 peak is also more intense than the experimental 78.2 line. Furthermore the $P_{68.8}$ line may also contribute to this peak. Our 103.6 line is much weaker than the experimental $I_{103.5}$ and conversely our 106.6 line is stronger than the experimental $I_{106.3}$. The $P_{94.7}$ line also contributes at almost the same energy as the $I_{103.5}$. In view of the fact that for example the 75.8 (theory) and 78.2 (experimental) phonons can differ by 2–3 meV, it does not seem implausible that our calculated 103.6 and 106.6 phonons should be interchanged for a proper indentification of the modes with experiment. Similarly, if the 95.5 and 96.7 lines in our calculation would be interchanged the spectrum would agree much better with experiment because the phonon with strong PL emission would then just add to what is already the strongest peak.

As already mentioned, it is striking that below $\sim$55 meV, the experimental peaks are all about a factor 10 smaller whereas in our calculation this is not the case. Besides this overall reduction of the peaks in experiment, there are other differences. Our strongest line in this region is at 35.9 with a weaker peak at (40.5,40.9 giving one peak) and another weaker one at 51.9. In contrast, in the

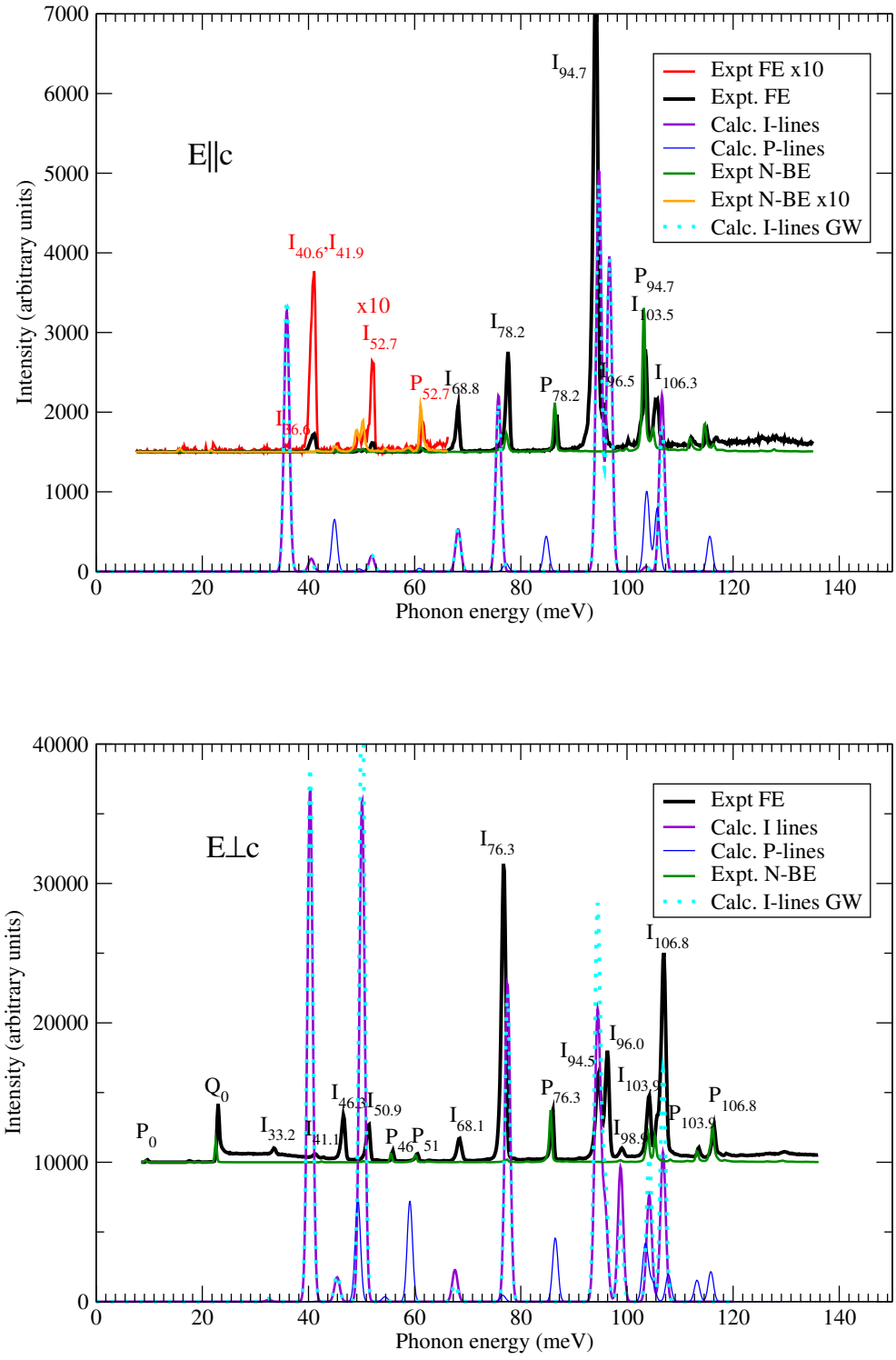

FIG. 6. The simulated photoluminescence spectra compared with experimental data (black lines). The experimental lines are offset vertically by an arbitrary amount. For $E \parallel c$ they correspond to Fig. 7c of Ref. 5 and for $E \perp c$ they correspond to Fig.7d. The dark green lines correspond to Fig. 7a ($E \parallel c$) and Fig. 7b ($E \perp c$) which were for samples with higher N doping emphasizing the P-lines. The violet lines (using LDA bands) and cyan dashed lines (using GW bands) are our calculated spectra based on Tables IV,V with a Gaussian broadening of 0.5 meV. The blue lines correspond to the LDA results but shifted up by 9 meV and represent the corresponding P-lines. For $E \parallel c$, the red and orange lines correspond to the experimental spectra $\times 10$ for the low phonon energy region. FE =Free exciton, N-BE is Nitrogen bound exciton

experiment, the strongest peak is the combined $I_{40.6,41.9}$ one and a relatively strong $I_{52.7}$ but quite weak $I_{36.6}$. Again, although the phonon energies seem to match well, there appear to be switches of these modes between theory and experiment when one takes into account the relative intensities.

Next, we move on to the $E \perp c$ polarization. In the experimental results, the highest peak is at 76.3 meV. In the calculation this peak is at 77.5 meV. The $I_{68.1}$ peak nicely agrees with our 67.6 mode. In the experiment, there are two sets of close peaks $I_{94.5}$, $I_{96.0}$ and $I_{103.9}$, $I_{106.8}$ with a weaker one $I_{98.9}$ in between. In our calculations there is peak corresponding to the combination of the 94.3, 94.8 meV phonons which is very strong followed by a weaker 95.9 meV one. The peaks at 104.2 and 106.8 agree well with the experimental ones in terms of the relative intensity. Overall the match in this region is fairly good, when also including the corresponding simulated P-lines. Again, it is remarkable that the peaks below 55 meV are reduced by a factor of at least 5 with respect to the higher phonon energy ones in the experiment. In contrast, in the theory, the two strongest peaks occur in this energy range. The experiment in this regon shows two weak peak at $I_{33.2}$ and $I_{41.1}$ followed by two larger peaks at $I_{46.3}$ and $I_{50.9}$. In the theory we also find a weak 32.5 peak but we find a strong 40.3 and 50.1 peak with a weaker 45.4 in between. Comparing this with the experiment, it appears that our calculated 40.3 should be identified with the experimental 46 meV phonon and our calculated 45.4 should be identified with the experimental 41.1 meV phonon so that their relative intensities would match.

Thus apart from the overall reduction factor of the PL replica with energies less than 55 meV in the experiment, there is a reasonable agreement in the relative intensities of the different phonon replicas when we take into account an uncertainty of a few meV on our calculated phonons which could lead to some interchanges compared to experiments in terms of mode ordering. The polarization dependence is also well described by the theory. This is an indication that the overall computational approach is valid and the matrix elements involved and energy band differences involved are sufficiently accurate. It is thus difficult to explain why our calculated intensities would be in error by a factor 5-10 for phonon energies less than 55 meV but not above this energy cut-off. Therefore we look for an alternative explanation for this in terms of another recombination channel.

It is noteworthy that the N-donor binding on the hexagonal site energy is 53 meV [20], which is remarkably close to the dividing line between weak and strong lines. The P-lines in the experimental PL spectrum in fact correspond to donor-bound excitons for the N impurity in a hexagonal N-site. The Q-lines correspond to a N-donor on the cubic site and is deeper (about 100 meV). The relative intensity of the phonon replicas of the P- and Q-lines are discussed by Ivanov *et al.* [5]. Because the binding energy of the exciton to the shallower hexagonal N is weaker, its phonon replicas are stronger but the zero phonon line is weaker.

If we ignore the exciton binding energy for a moment and think in terms of free electrons recombining with free holes via combined electron-phonon and electron-photon interaction, then we need to also include the possibility of interacting with the available empty N-donor levels. If the phonon energy reduces the energy by less than the donor binding energy, then the electron could still get trapped by the donor and subsequently recombine via another phonon and interaction with the radiation field giving rise to the P-series of PL lines. However, if the energy loss due emitting a phonon is already larger than the donor binding energy, then it can no longer be trapped. Thus it would seem that for low phonon energies, there is another channel open in the decay process which is not available for higher phonon energies. To fully calculate the branching ratios of the different decay channels, including or not a donor trap level is beyond the scope of the present paper but at least it seems to provide a somewhat plausible explanation for the mismatch between theory and experiment in intensities of the indirect phonon mediated recombination below and above ~ 55 meV.

We note that at the low temperatures of the experiment (2K), in equilibrium, most donors should be neutral and not be able to capture an electron. However, the PL experiment has created at least some non-equilibrium to have excited electrons in the conduction band and holes in the valence band. Thus, there must then also be some non-equilibrium in the donor state state occupation and hence some donors should be in the ionized state and be able to capture and electron.

On the other hand, in terms of an exciton picture, we could think of the process as binding a free exciton to a neutral donor before it recombines. Although this binding energy is less than the donor binding energy (about 9 meV as mentioned earlier) this results from the more complex interactions in the four-particle center consisting of the donor, the electron it binds and a conduction electron and valence band hole already bound into an exciton state. It is somewhat less clear why the donor binding energy provides the limiting energy for the two type of processes in this picture but the essence remains the same: there is a decay channel for indirect recombination involving only an emitted phonon and a photon and another channel for an additional interaction of the exciton with a donor, which is only available if the phonon does not already carry away too much of the energy. The branching ratio of these two distinct processes should determine the relative intensities of the P compared to the I lines for a given concentration of donors.

Our assumption would predict that below the 55 meV cut-off the ratio of the P-lines to the I-lines should be higher than above it. Because of the overlap of I and P-lines this is rather difficult to ascertain. We pick the well separated $I_{76.3}/P_{76.3}$ ratio which from the areas under the curve we estimate to be about 7 while for the

$I_{46.3}/P_{46.3}$ it is $\sim$ 2.5. Thus the P-lines are indeed stronger relative to the I-lines below 55 meV.

Note that we cannot directly compare intensities with the differential absorption spectra of Klahold *et al.* [6] because these correspond to $d\alpha/d\lambda$ the wave length derivative of the absorption coefficient.

IV. CONCLUSION

In this work, we simulated the PL sepctra due to the recombination of a free exciton at low tempeature for the indirect gap semiconductor 4H SiC from first-principles calculations. The phonon frequencies and the polarization dependence of which phonons occur for which polarization, which is essentially explained by group theory are in excellent agreement with available experiment results.[5] The relative intensities which depend on the actual matrix elements is also in fair agreement if we allow some closely lying phonon modes to be interchanged so that their intensities match better to experiment. In other words, we match which phonon matches a particular experimental replica peak not only on the basis of the best match in phonon frequency value but also on their relative intensities and their polarization. However, the free exciton lines corresponding to phonons with frequency below $\sim$ 55 meV appear to be suppressed in the experiment by a factor 5–10. We explain that observation in terms of a competition with trapping the electron or exciton first at the donor when the phonon energy is less than the donor binding energy. The relative intensities of the phonon replica were shown not to depend strongly on the GW corrections to the bands.

Appendix A: Optical Matrix elements

The non-zero optical dipole matrix elements connecting to the CBM at M are given in Table VI. It is interesting to note that only a few states have significantly larger matrix elements than the other ones.

ACKNOWLEDGMENTS

We thank Prof. Robert P. Devaty for helpful discussions and Prof. Ivan G. Ivanov for sending us the digitized experimental data used in Fig. 6. This work was supported by the U.S. Department of Energy – Basic Energy Sciences, under grant No. DE-SC-0008933. Calculations made use of the High Performance Computing Resource in the Core Facility for Advanced Research Computing at Case Western Reserve University.

[1] L. Patrick, W. J. Choyke, and D. R. Hamilton, Phys. Rev. **137**, A1515 (1965).
[2] W. R. L. Lambrecht, S. Limpijumnong, and B. Segall, in *Silicon Carbide and Related Materials 1995: Proceedings of the Sixth International Conference, Kyoto 1995*, Institute of Physics Conference Series, Vol. 142, edited by S. Nakashima, H. Matsunami, S. Yoshida, and H. Harima (1996).
[3] M. Hofmann, A. Zywietz, K. Karch, and F. Bechstedt, Phys. Rev. B **50**, 13401 (1994).
[4] W. J. Choyke, R. P. Devaty, L. L. Clemen, M. F. MacMillan, and Y. M, in *Silicon Carbide and Related Materials 1995: Proceedings of the Sixth International Conference, Kyoto 1995*, Institute of Physics Conference Series, Vol. 142, edited by S. Nakashima, H. Matsunami, S. Yoshida, and H. Harima (1996).
[5] I. G. Ivanov, U. Lindefelt, A. Henry, O. Kordina, C. Hallin, M. Aroyo, T. Egilsson, and E. Janzén, Physical Review B **58**, 13634 (1998).
[6] W. M. Klahold, W. J. Choyke, and R. P. Devaty, in *Silicon Carbide and Related Materials 2017*, Materials Science Forum, Vol. 924 (Trans Tech Publications Ltd, 2018) pp. 239–244.
[7] J. Noffsinger, E. Kioupakis, C. G. Van de Walle, S. G. Louie, and M. L. Cohen, Phys. Rev. Lett. **108**, 167402 (2012).
[8] C. Aversa and J. E. Sipe, Phys. Rev. B **52**, 14636 (1995).
[9] F. Giustino, Rev. Mod. Phys. **89**, 015003 (2017).
[10] X. Gonze, J. M. Beuken, R. Caracas, F. Detraux, M. Fuchs, G. M. Rignanese, L. Sindic, M. Verstraete, G. Zerah, and F. Jollet, Computational Materials Science **25,3**, 478 (2002/11).
[11] C. Hartwigsen, S. Goedecker, and J. Hutter, Phys. Rev. B **58**, 3641 (1998).
[12] M. van Schilfgaarde, T. Kotani, and S. Faleev, Phys. Rev. Lett. **96**, 226402 (2006).
[13] T. Kotani, M. van Schilfgaarde, and S. V. Faleev, Phys.Rev. B **76**, 165106 (2007).
[14] L. Hedin, Phys. Rev. **139**, A796 (1965).
[15] L. Hedin and S. Lundqvist, in *Solid State Physics, Advanced in Research and Applications*, Vol. 23, edited by F. Seitz, D. Turnbull, and H. Ehrenreich (Academic Press, New York, 1969) pp. 1–181.
[16] C. Bhandari, M. van Schilgaarde, T. Kotani, and W. R. L. Lambrecht, Phys. Rev. Materials **2**, 013807 (2018).
[17] C. Persson and U. Lindefelt, Journal of Applied Physics **82**, 5496 (1997).
[18] O. Madelung, ed., *Semiconductors* (Springer Berlin Heidelberg, 1991).
[19] W. Klahold, C. Tabachnick, G. Freedman, R. P. Devaty, and W. J. Choyke, in *Silicon Carbide and Related Materials 2016*, Materials Science Forum, Vol. 897 (Trans Tech Publications Ltd, 2017) pp. 250–253.
[20] A. O. Evwaraye, S. R. Smith, and W. C. Mitchel, Journal of Applied Physics **79**, 7726 (1996).

TABLE VI. Optical dipole matrix elements of z, x, y at the M point (along x-axis) connecting to the M_4 CBM. For each matrix element the band number is indicated and on top the symmetry-label of these bands is indicated.

	band	z	band	x	band	y
symmetry	M_4		M_1		M_3	
	2	-0.0356	1	-0.0283	12	-0.4753
	3	-0.0257	4	0.0192	13	0.1814
	5	0.0552	6	0.2121	28	0.1104
	8	-0.2383	7	0.0530	29	-0.1682
	10	-0.0546	9	-0.3071	39	-0.0116
	14	0.4705	15	0.1793	40	0.0783
	19	0.1041	18	0.0107		
	21	-0.0144	20	0.0935		
	25	-0.0802	22	0.0485		
	26	0.1762	24	-0.0977		
	30	-0.0854	27	-0.0294		
	33	-0.0243	31	-0.0072		
	37	0.0713	34	-0.1072		
			35	0.0644		
			36	0.0368		